MEAN FLOW AND TURBULENT STATISTICS OF THE FLOW OVER A SUBMERGED SHARP-CRESTED WEIR.

CHAEWOONG BAN
Ph.D. student, Department of Civil and Environmental Engineering, Yonsei University, Seoul, Republic of Korea, blue8803@yonsei.ac.kr

SUNG-UK CHOI
Professor, Department of Civil and Environmental Engineering, Yonsei University, Seoul, Republic of Korea (corresponding author), schoi@yonsei.ac.kr

ABSTRACT

Flow over a sharp-crested weir shows the free flow, for which the critical flow occurs at the tip of the weir. However, during the high flow, the downstream water level affects the overflow and the flow over the weir becomes the submerged flow. The submerged flow exhibits four different flow regimes depending on the downstream water level, namely impinging jet, surface jump (or breaking wave), surface wave, and surface jet. In this paper, the four flow regimes of the submerged flows over the sharp-crested weir are simulated using large eddy simulation (LES). The flow condition comes from the laboratory experiment by Rajaratnam and Muralidhar (1969), and the computed results are validated against experimental data of the surface jet. For the same discharge, the impinging jet, surface jump, and surface wave are made by changing the ratio of the tailwater depth and the head above the weir crest. Characteristics of the free surface fluctuations, and mean flow and turbulence statistics of the four flow regimes are investigated. LES results indicate that the four flow regimes show distinctive characteristics of the recirculation zones downstream of the weir and the free surface. Their impact on the bed downstream of the weir is also examined.

Keywords: *Weir, Submerged flows, Large eddy simulation, Mean flows, Turbulent statistics*

1. INTRODUCTION

Flow over a sharp-crested weir shows the free flow, where the critical flow occurs at the tip of the weir. However, as the discharge increases, the downstream water level affects the overflow and the flow over the weir becomes the submerged flow. Wu and Rajaratnam (1996) divided the submerged flow into impinging jet (Figure 1(d)) and surface flow regimes (Figures 1(a)-1(c)). For the impinging jet regime, the flow over the weir plunges into the tailwater, diffuses as a plane submerged jet, and eventually hits the bed of the downstream channel. For the surface flow regime, the flow remains as a jet at the surface in the downstream channel, with its thickness increasing downstream due to turbulent mixing. Surface flow regimes can further be classified into the surface jump (or breaking wave), surface wave, and surface jet.

Wu and Rajaratnam (1996) proposed a criterion to distinguish the impinging jet and the surface flow. The following relationships present the transition region from impinging jet to surface flow:

$$t/h = 1 - 0.215\lambda + 0.0142\lambda^2 - 0.00031\lambda^3 \text{ (for lower curve)} \quad (1)$$

$$t/h = 1 - 0.126\lambda + 0.0076\lambda^2 - 0.00017\lambda^3 \text{ (for upper curve)} \quad (2)$$

which are the lower and upper bounds of the transition, respectively. In Eqs. (1) and (2), $\lambda = \sqrt{g(h-t)/((q/y_t))}$, g = gravitational acceleration, h = head above the crest of the weir, t = depth of tailwater above the weir crest, q = unit discharge, and y_t = tailwater depth. The region between the upper curve and lower curve indicates the transition stage, where the flow regime is affected by the history of the flow, so-called the hysteresis effect. Azimi et al. (2016) also presented classification of submerged flows for $0.146 < h/P < 0.389$ based on t/h, where P = weir height. That is, impinging jet, surface jump, surface wave, and surface jet occur in the respective ranges of $t/h < 0.2$, $0.2 < t/h < 0.48$, $0.48 < t/h < 0.78$, and $t/h < 0.78$. The boundary between the surface wave and surface jet is defined when the amplitude of the wave becomes less than 10% of the approach flow head.

This research aims to study the flow characteristics of submerged flows over sharp-crested weirs in various flow regimes. The flows downstream of the weir are featured by highly 3D unsteady nature shed from the weir,

requiring highly-resolved large eddy simulation (LES) to demonstrate the detailed flow structures. This study presents results of the LES of four different flow regimes to investigate the mean flow and turbulent structures. Hydraulic conditions for the surface jet come from experiments by Rajaratnam and Muralidhar (1969). The other three flow regimes are made by satisfying the threshold proposed by both Wu and Rajaratnam (1996) and Azimi et al. (2016).

2. GOVERNING EQUATIONS

Filtered Navier-Stokes equations governing the resolved quantities in LES are solved using OpenFOAM (Open Field Operation and Manipulation, Weller et al., 1998). The filtered Navier-Stokes equations are given by

$$\frac{\partial \bar{u}_i}{\partial x_i} = 0 \tag{3}$$

$$\rho \frac{\partial \bar{u}_i}{\partial t} + \rho \bar{u}_j \frac{\partial \bar{u}_i}{\partial x_j} = -\frac{\partial \bar{p}}{\partial x_i} + \frac{\partial}{\partial x_j}\left(\bar{\tau}_{ij} + \tau_{ij}^{SGS}\right) \tag{4}$$

which are the conservation laws for mass and momentum, respectively. In. Eqs.(3) and (4), x_i is Cartesian coordinates (i = 1, 2, 3 corresponding to x, y, and z directions, respectively), t is the time, ρ is the fluid density, $\bar{u}_i$ is the instantaneous velocity vector, $\bar{p}_i$ is the filtered pressure, $\bar{\tau}_{ij}$ ($= \rho\nu\partial\bar{u}_i/\partial x_j$) is the filtered stress tensor associated with viscosity, and τ_{ij}^{SGS} ($= \rho\left(\bar{u}_i\bar{u}_j - \overline{u_i u_j}\right)$) is the subgrid-scale (SGS) stress tensor. The SGS stress tensor means the effect of the unresolved, small-scale turbulent motion, and this term is comprised of isotropic and anisotropic components. Using the eddy-viscosity concept, the anisotropic part of the SGS stress tensor can be presented by

$$\tau_{ij}^{SGS} = \rho\left(\bar{u}_i\bar{u}_j - \overline{u_i u_j}\right) = 2\rho\nu_t\bar{S}_{ij} + \frac{1}{3}\delta_{ij}\tau_{kk}^{SGS} \tag{5}$$

where ν_t is the kinematic eddy viscosity, δ_{ij} is the Kronecker delta, and $\bar{S}_{ij} = 1/2\left(\partial\bar{u}_i/\partial x_j + \partial\bar{u}_j/\partial x_i\right)$ is the filtered strain rate tensor. In the present study, the SGS stress tensor is modeled by the wall-adapting local eddy viscosity (WALE) model, proposed by Nicoud & Ducros (1999).

In the computations, three computational grids were used, namely coarse, intermediate, and fine grids for the surface jet case, and fine grids for the other cases. For the fine grid resolution, the maximum grid spacing is Δ = 5 x 10^{-3} m. In the near-wall region, the grid size is Δ = 2.5 x 10^{-3} m with a spatial average of $\Delta^+ \cong 13$. The number of grid cells is about 10.8 x 10^6 for the fine grid. The inflow condition comes from a preliminary LES computation in a periodic channel of an identical cross-section. The velocity fields did not include fluctuations, but time-averaged velocity fields were fed into the inflow due that the weir obstruction is the major factor in the formation of the turbulence eddies. For the free surface tracking, volume of fluid (VOF) method is used. In the VOF method, the transport equation for the VOF function, α, of each phase is solved simultaneously with a single set of mass and momentum equations for the whole flow field. In the simulation result, interface corresponding α = 0.5 is considered as free surface.

The flow conditions are obtained from the laboratory experiment for the surface jet by Rajaratnam & Muralidhar (1969). The bulk velocity and approach flow depth are 0.0741 m/s and 0.141 m, respectively, and the height of the weir is 0.302 m. This yields Reynolds number and Froude number of 11,170 and 0.061, respectively.

3. RESULTS

Figure 2 shows time-averaged streamwise velocity profiles at various locations from the LES results and measured data by Rajaratnam & Muralidhar (1969). The velocity profiles show that the flow accelerates by passing over the weir and the backward flows occur near the bed. It can be seen that the overall agreement between the simulated velocity profiles and measured data is good. In addition, three different grid resolutions are tested and Figure 2 confirms that the fine-mesh grid is accurate enough to converge the solution.

Figure 3 presents contours of time-averaged streamwise velocity with streamlines for the four different flow regimes. The LES results show that the characteristics of the recirculation zones and the free surface downstream of the weir are entirely different depending on the flow regime. For the surface jet in Figure 3(a), a jet is made at the tip of the weir, forming a large primary vortex with a small weak vortex at the lower corner of the re-circulation zone. The contour plot indicates that reattachment takes place at x/P = 7.6. As t/h decreases, the surface wave is generated as can be seen in Figure 3(b). The jet flow becomes more intensive with the flow depth reduced over the tip of the weir. This resulted in stronger backward flows, increasing the size of the weak vortex at the lower corner. Figure 3(c) shows the surface jump, which is made as t/h decreases from the surface wave. The generation of the surface jump is confirmed by the presence of the surface vortex. Strong backward

flows are observed in the vicinity of the bed. If *t*/*h* further decreases, then the impinging jet is generated. The overflow is heading the bed, with counter-rotating vortices formed about the overflow. The size of the weak vortex at the lower corner is observed to be larger than that of the weak vortices made in the other three flow regimes.

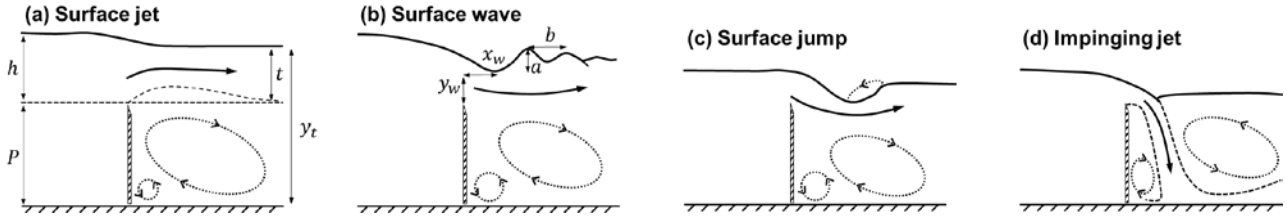

Figure 1. Classification of submerged flow regimes.

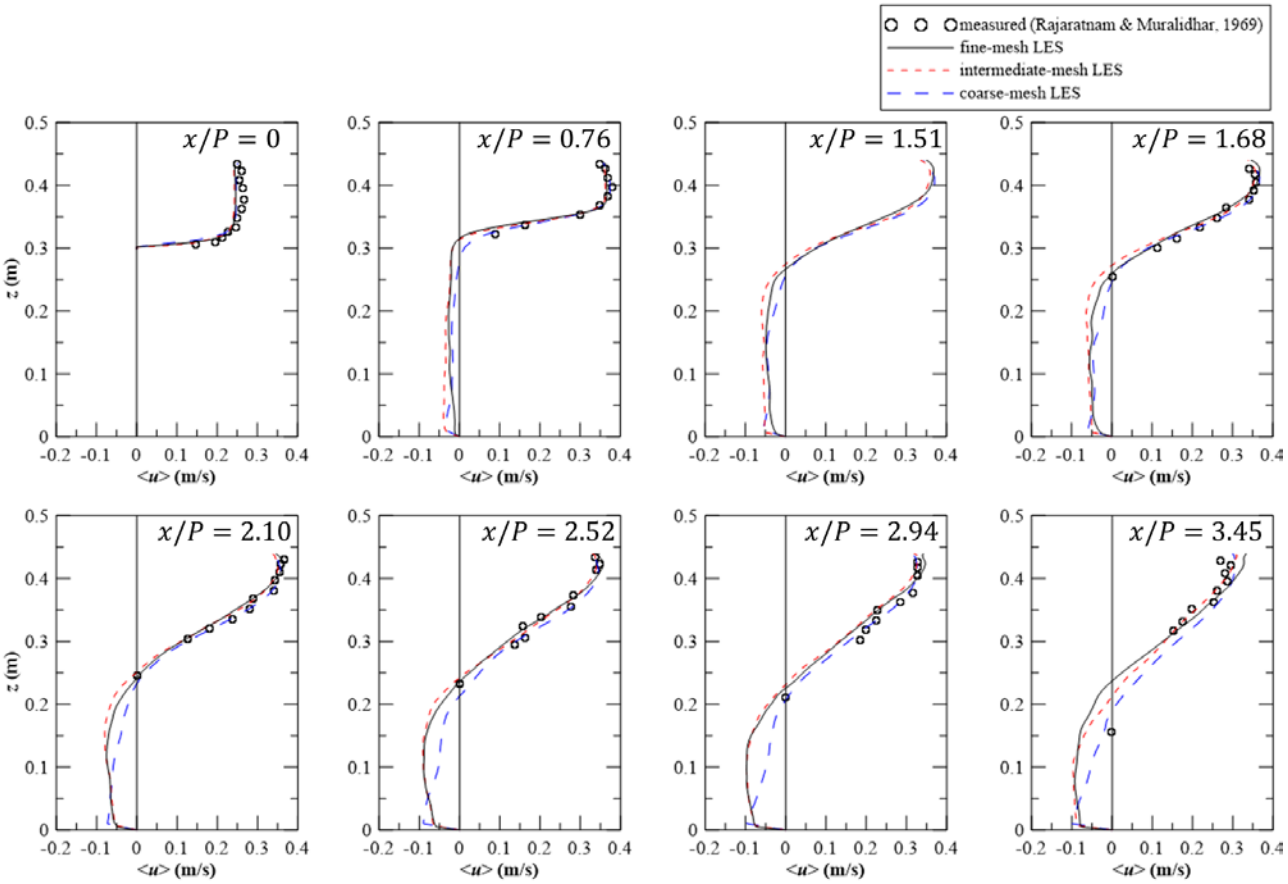

Figure 2. Time-averaged streamwise velocity profiles along the streamwise direction.

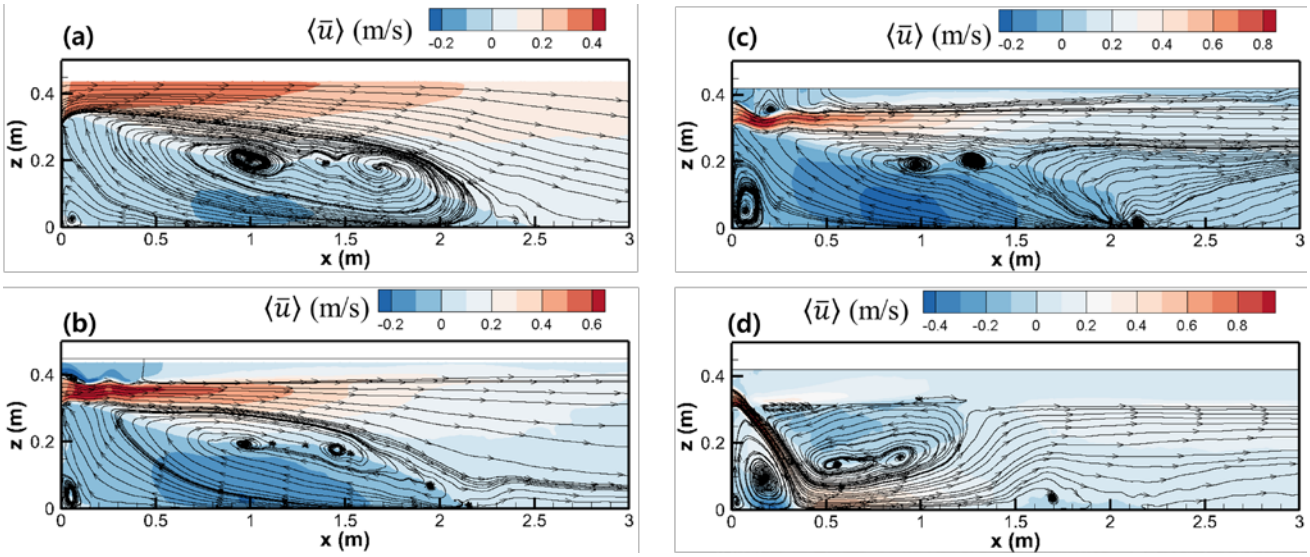

Figure 3. Contours of time-averaged streamwise velocity with streamlines: (a) surface jet; (b) surface wave; (c) surface jump; (d) impinging jet.

4. CONCLUSIONS

Large eddy simulation was carried out for turbulent flows over a submerged weir. Four different overflows, namely surface jet, surface wave, surface jump, and impinging jet, were simulated. The LES results were compared with the measured data by Rajaratnam & Muralidhar (1969), showing good agreement. Distinctive characteristics of the recirculation zones and the free surface were found and discussed.

ACKNOWLEDGMENTS

This work was supported by the National Research Foundation of Korea (NRF) grant funded by the Korea Government (NRF2017R1A2A2A05069836).

REFERENCES

Azimi, A. H., Rajaratnam, N., and Zhu, D. Z. (2016). Water surface characteristics of submerged rectangular sharp-crested weirs. *Journal of Hydraulic Engineering*, 142(5), 06016001.

Nicoud, F., and Ducros, F. (1999). Subgrid-scale stress modelling based on the square of the velocity gradient tensor. Flow, *Turbulence and Combustion*, 62(3), 183-200.

Rajaratnam, N., and Muralidhar, D. (1969). Flow below deeply submerged rectangular weirs. *Journal of Hydraulic Research*, 7(3), 355-374.

Weller, H. G., Tabor, G., Jasak, H., and Fureby, C. (1998). A tensorial approach to computational continuum mechanics using object-oriented techniques. *Computers in Physics*, 12(6), 620-631.

Wu, S., and Rajaratnam, N. (1996). Submerged flow regimes of rectangular sharp-crested weirs. *Journal of Hydraulic Engineering*, 122(7), 412-414.